Thong Duc Hong
Ho Chi Minh City University of Technology (HCMUT)
Vietnam National University Ho Chi Minh City (VNU-HCM)
Vietnam

Phat Tan Truong
Ho Chi Minh City University of Technology (HCMUT)
Vietnam National University Ho Chi Minh City (VNU-HCM)
Vietnam

Minh Quang Pham
Ho Chi Minh City University of Technology (HCMUT)
Vietnam National University Ho Chi Minh City (VNU-HCM)
Vietnam

Hoa Nam Ho
Ho Chi Minh City University of Technology (HCMUT)
Vietnam National University Ho Chi Minh City (VNU-HCM)
Vietnam

Hoang Minh Do Le
Ho Chi Minh City University of Technology (HCMUT)
Vietnam National University Ho Chi Minh City (VNU-HCM)
Vietnam

Thang Viet Vu
Ho Chi Minh City University of Technology (HCMUT)
Vietnam National University Ho Chi Minh City (VNU-HCM)
Vietnam

Design, Development and Manufacture of a Small Electric Motor Dynamometer

Studying electric vehicle performance, operating range, and control algorithms is still limited in developing countries because it requires specialized equipment, while electric vehicles are increasingly widely used, such as electric cars, electric motorbikes, electric bicycles, etc. This paper introduces the design and manufacture of a small electric motor dynamometer, especially the in-wheel motor. Based on the performance of electric motors and the alternator characteristics, the chain drive was cautiously analyzed and designed to investigate different electric motor speed characteristics over their entire operating range. Especially in this study, the chain drive has three stages with transmission ratios of 1/4, 1/3, and 1/2.5. Besides, a controller that can automatically adjust the electric load level to determine various motor characteristics under constant load and throttle settings is also designed to control the dynamometer and collect essential data. Furthermore, the graphic user interface is built to operate the dynamometer quickly and flexibly. With a flexible transmission ratio and a comprehensive algorithm control, the dynamometer can investigate various characteristics of electric motors used for popular motorbikes and bicycles with power up to 3000W. The designed dynamometer not only has a compact design, stable operation, and affordable price but is also easy to assemble, operate, and maintain. These findings can be applied to develop the dynamometer to investigate the performances of the electric motor and its auxiliary system, serving the research and development process of electric motorbikes used in developing countries today.

Keywords: *electric motor, dynamometer, alternator, motor testing, motor performance.*

1. INTRODUCTION

Nowadays, the population explosion around the world has led to an increasing demand for transportation, which has led to the dramatic depletion of fossil fuels and thereby caused global warming due to the greenhouse effect. To solve this problem, developed countries have switched to using electric vehicles. In developed countries with good transport infrastructure, research and development of electric cars are interesting and promoted. Not out of that trend, developing countries are also gradually switching to using electric bicycles and electric motorbikes due to their suitability to the conditions of these countries.

The issue that needs to be considered in using electric vehicles is optimizing the energy used to improve performance and, most importantly, extending the vehicle's operating range [1–5]. In order to achieve this objective, the characteristics of the electric motor need to be determined, through which it is possible to easily develop auxiliary devices (System Integration, controller, etc.), as well as control algorithms for each operating condition on the road [6]. To assist in measuring the performance characteristics of electric motors, using motor test benches or chassis test benches is a beneficial solution. Using test benches brings many benefits, such as describing the motor characteristics at several conditions and repeating the experiment under uniform and stable conditions. However, owning a commercial test bench with full features is very expensive. Therefore, some researchers have presented the design and implementation process of the dynamometer used for electric motors to solve some specific characteristics. He et al. [7] designed a test bench for the electric wheel of vehicles (the vehicle with an electric motor in the wheel hub) to simulate the actual interaction between the electric wheel and the roads. Except for the electric dynamometer, the roller and flywheel are used to simulate inertia when running. Hassan et al. [8] designed a simple chassis dynamometer for two-wheel electric vehicles to examine the torque and power versus the vehicle's speed. However, the test bench only used the roller to create the load and did not have any controller to adjust the load act in the vehicle. Su et al. [9] designed and fabricated a chassis dynamometer for testing electric vehicles, with an adjustable load system to simulate different vehicle resistance when running in practice, such as constant-speed drive, braking, accelerating, and running downhill.

Received: November 2024, Accepted: December 2024
Correspondence to: Thong Duc Hong, Ho Chi Minh City University of Technology, Ly Thuong Kiet Street 268, District 10, Ho Chi Minh City, Vietnam
E-mail: hongducthong@hcmut.edu.vn
doi: 10.5937/fme2501001H

In another aspect, brushless direct current motor (BLDC) is the main propulsion for all-electric vehicles today; they are widely used for any electric vehicle, from electric cars and electric buses to especially electric bicycles and electric motorbikes, because of their benefits (high-performance, fuel cost savings, easy maintenance, and repair [10–13]. There have also been studies on the characteristics of this type of electric motor. Racewicz et al. [14] designed and implemented a light two-wheeled electric vehicle using a 3 kW BLDC motor and then used a dynamometer to test its power, torque, and speed. The resulting data is used to calculate the average working range of the bike. Consequently, it can travel the average theoretical range of approximately 80 km with a 27.5 Ah battery, which is just a 12.5% difference from the road tests. Kolator et al. [15]used a MAHA LPS 3000 chassis dynamometer with additional designed instruments to test the traction parameters of the lightweight two-wheeled electric vehicle in both laboratory and road conditions. As a result, they have successfully created the methodology for testing this type of vehicle. Kang and Kim [16] proposed a new drive performance test method to determine the road load for e-bikes that use in-wheel BLDC motors by measuring the motor's current consumption and utilizing the relationship between the motor's torque and current at constant speed.

It can be seen that the study on the characteristics of small electric motors is essential in developing electric vehicles, while the commercial test bench models are costly. In addition, the publications related to the design and research of small electric motor dynamometers are limited. Therefore, it is necessary to study small electric motor dynamometers suitable for electric bicycles and electric motorbikes with the criteria of simplicity, accuracy, stability, and reasonable price, especially in developing countries, because the cost of this equipment is often remarkably high.

In this study, a small electric motor dynamometer is designed and manufactured to meet the increasing demand for electric motor performance research. A design research process is proposed for an electric dynamometer with a simple structure and low cost, but it still meets the requirements for studying the various characteristics of the wheel hub motor. A control system combining microprocessors and computer software is designed to flexibly control the electric load, suitable for surveying the entire characteristics of the electric motor under many operating modes (including full-load and part-load). Based on the study's results, the features of small electric vehicles have been developed and improved to become more accessible. They will create a premise for developing countries such as Vietnam, Indonesia, and Laos to participate in this new field.

2. MATERIALS AND METHODS

2.1 General layout diagram of electric motor dynamometer

The schematic diagram of the dynamometer system is illustrated in Figure 1. The electric motor test bench consists of a BLDC and driver, drivetrain, alternator, electrical load system, power supply, and controller; all these components are arranged on the test bench frame. The controller also includes several other devices, such as a static torque sensor and transmitter, BLDC input power monitor, and computer to take responsibility for controlling the dynamometer and collecting data.

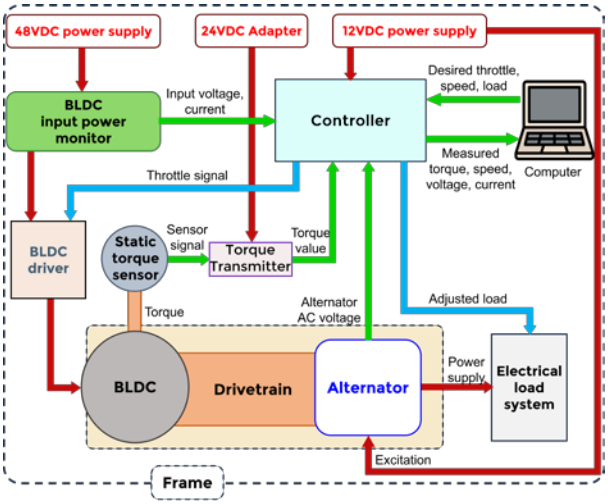

Figure 1. Schematic diagram of the dynamometer used for small electric motor.

The working principle of this dynamometer is based on the generator dynamometer type [17]. The testing BLDC will drive the alternator through the drivetrain. When the alternator operates, it creates electric power to supply to the electrical load system, consuming the electric motor's output power. The resistance of the alternator acting on the motor changes when the electric load level varies. Therefore, the operating point of certain electric motor characteristics can be determined by controlling the electric load level. In this study, the electric load level can be automatically controlled by the controller to determine the desired motor characteristics. When the dynamometer is operating, the desired operating point of the motor is set by setting the throttle percentage and desired motor speed on the graphics user interface of the computer (GUI). By comparing the desired speed with the measured speed, which is obtained from the alternator AC voltage frequency, the controller will calculate how much the electric load level is required to keep the motor operating at the desired point. The computer and the controller are set to communicate, so it is easy to control the dynamometer and collect data from the computer. The power supply system consists of a 48VDC battery for the BLDC, a 12VDC battery for the controller and excitating the alternator, and a 24VDC adapter used by the torque transmitter.

2.2 Components of electric motor dynamometer

The components of the dynamometer are preliminarily determined as follows:

- This study designs and applies two motors integrated into wheels, such as the Golden Motor MP4 – 24V – 15A50T and the Lunyee TX48 – 48V BLDC wheel hub motor with the power of 200W and 1000W. In this study, the alternator of the automobile – a synchronous generator is used,

which is very popular, affordable, stable, and has suitable power.

- Designing the load system for the dynamometer requires the load system to accommodate the power range of the components involved, enabling flexible testing scenarios. Among the options for the electrical consumer unit, the headlight bulb is a practical choice due to its compact size, variety of types for varying loads, and ease of load control.
- The controller collects data (alternator AC voltage frequency, motor torque, input voltage, input current, etc.) and uses the data to control the operation of the test bench. The motor speed is determined based on the alternator frequency and the transmission ratio. Torque is determined by a static torque sensor and a transmitter installed directly on the shaft of the electric motor. The controller needs to perform many tasks simulta–neously, including collecting desired speed and throttle, measuring actual speed and torque, calcu–lating the required electric load, setting the throttle, and controlling the electrical load system to balance the generated power of the motor. There–fore, the STM8S208C6T6 – Performance line microcontroller of the STM8S series is selected for this application. It features a full set of peripherals and provides performance for medium-to-high-end applications, including 10-bit ADC to measure analog signals such as voltage and current, Timer – PWM to control the electrical load and simulate throttle signal, Timer – Input Capture to measure speed, UART to communicate with the torque transmitter and the computer.
- LabVIEW software is used to program the inter–face to communicate with the controller, allowing control of the operation of the dynamometer and collecting data such as speed, torque, and power of the motor.
- The automotive alternator is used to create the load for the BLDC wheel hub motor, leading to signi–ficant differences in their speed ranges. Also, the BLDC wheel hub motor's speed is measured thro–ugh the alternator's frequency. Thus, a drivetrain system with a flexible transmission ratio and limited rotating speed slip is required. Therefore, the chain drive is designed circumspectly to match the operating range between these two components.
- The dynamometer frame is carefully designed to provide places for attaching components and ensure that all the details, clusters, and systems do not overlap and collide, which is first created by a 3-D model to visualize the overall design before implementing the frame. In addition, polycarbonate sheets with high impact, lightweight, and aesthetics are chosen to cover all of the boundary surfaces of the dynamometer, forming a protective layer that separates the system from the outside.

3. CALCULATIONS AND TECHNICAL DESIGN OF ELECTRIC MOTOR DYNAMOMETER COMPONENTS

3.1 Electric motor

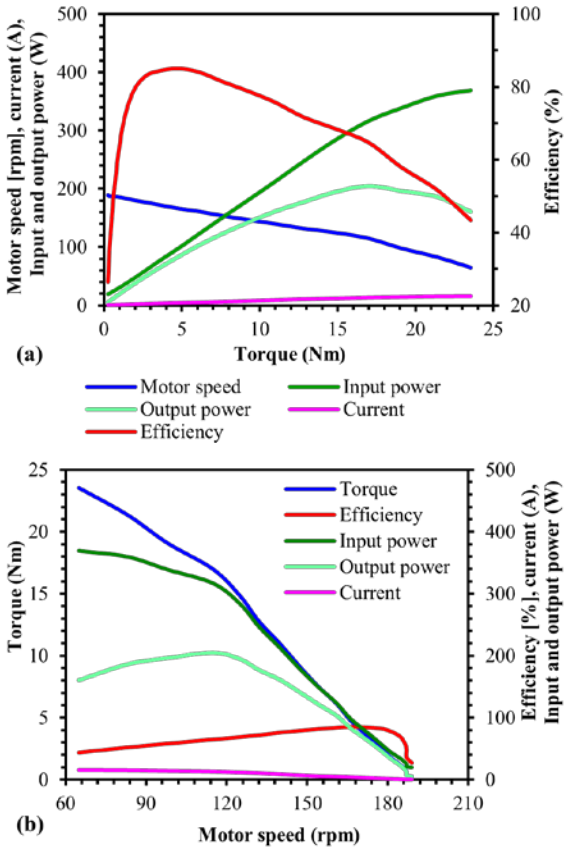

Figure 2. Golden Motor MP4 24V – 200W BLDC wheel hub motor performance curves: (a) varies with torque, (b) varies with motor speed [18].

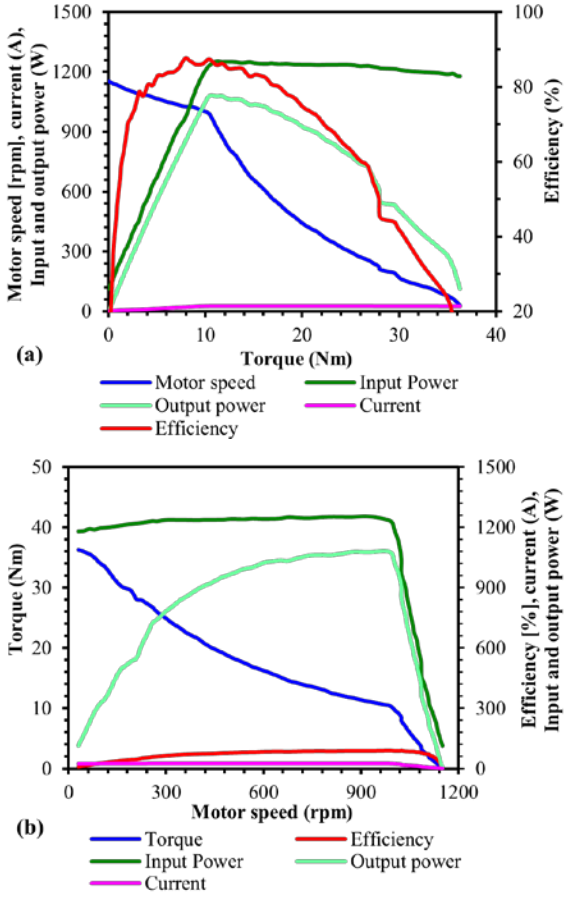

Figure 3. Lunyee TX48 48V – 1000W BLDC wheel hub motor performance curves: (a) varies with torque, and (b) varies with motor speed [19].

In this section, the Golden Motor MP4 – 24V – 15A50T and the Lunyee TX48 – 48V BLDC wheel hub motor with the power of 200W and 1000W, respectively, are selected as representatives to consider for the design calculation of this study.

Note that other BLDC wheel hub motors with the same power output will also give performance curves almost similar to the two selected BLDC wheel hub motors above. The performance curves of these motors are depicted in Figure 2a and Figure 2b, correspon–dingly.

Figure 2 illustrates that the highest output power occurs when torque reaches the value of about 17 Nm, corresponding to the motor speed of approximately 115 rpm. In order to achieve the highest output power, more than 300 W of electric input power is required. The maximum electric input power that the motor consumes can be up to 370W, which is also when the torque of the motor reaches its peak at 23.5 Nm with the motor's rotational speed of 70 rpm.

As shown in Figure 3, the maximum torque of the TX48 48V-1000W BLDC wheel hub motor is nearly 36 Nm, with an electric power supply of roughly 1200 W at about 50 rpm of motor speed. On the other hand, the output power of this motor reaches the highest point when the torque of the motor is about 10 Nm at the motor rotational speed near 1000 rpm, which needs almost 1250 W of electric input power.

3.2 Alternator

In this research, the Delco Remy 12SI – 12V – 78A alternator is selected to use in the dynamometer system, and its performance curve is shown in Figure 4. This alternator has an operating speed range from 1000 – 8000 rpm and produces stable output power between 1000 W and 1100 W at an operating speed range of about 4000 to 8000 rpm. With such an output power range, this alternator needs to receive input power from 2400 to nearly 3000 W.

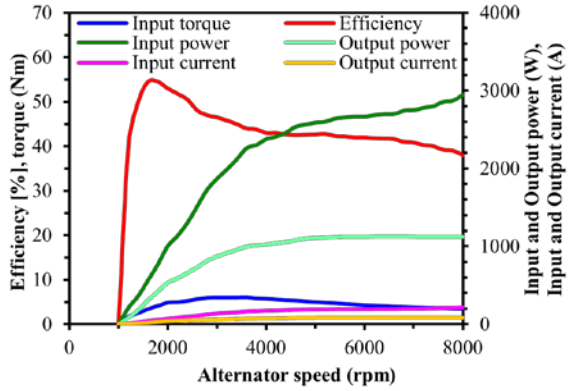

Figure 4. Delco Remy 12SI – 12V – 78A alternator performance curve [20].

3.3 Correlation between electric motor perfor–mances with torque and power at alternator shaft

The alternator's operating speed range is from 1000 to 8000 rpm while the Golden Motor MP4 – 24V – 15A50T and the Lunyee TX48 – 48V BLDC wheel hub motor's operating speed range are from 0 to 300 rpm and from 0 to 1100 rpm, respectively. Hence, to ensure that the alternator can work properly and consumes the motor's generated power at all operation points, the authors have selected the transmission ratio at 4, 12, and 30 to visualize the correlation between the electric motor and alternator performance.

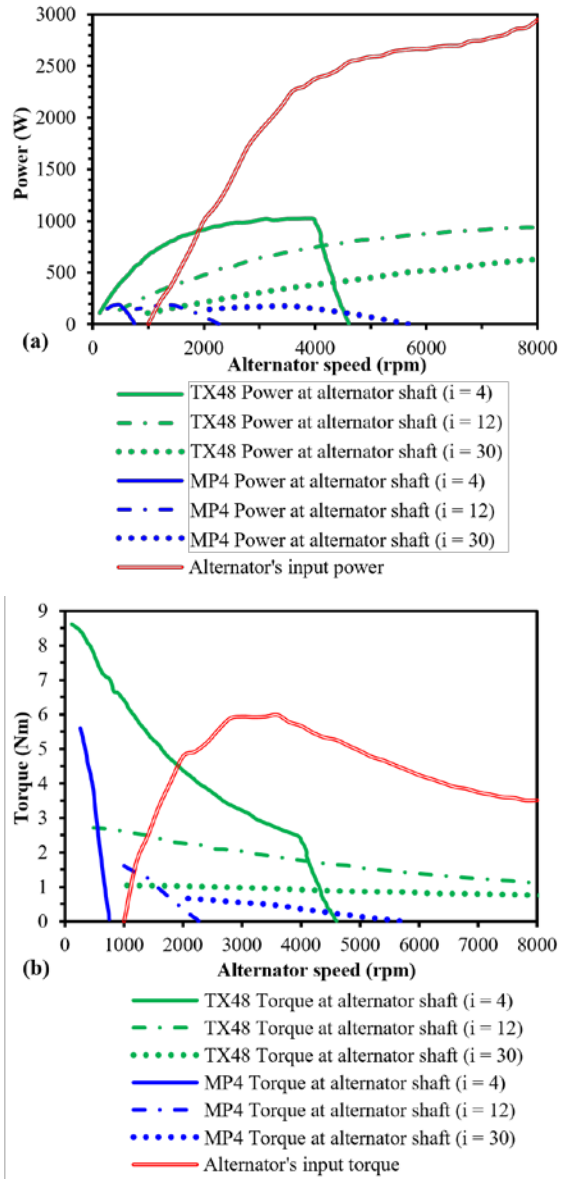

Figure 5. Correlation between BLDC wheel hub motor and alternator performance curves along with (a) torque and (b) power.

The correlation between electric motor and alter–nator performance curves, related to torque and power, is shown in Figure 5. The performance curves of both BLDC wheel hub motors at the transmission ratios of 4, 12, and 30 at the alternator's shaft, respectively, are illustrated to visualize the capability of the alternator to develop sufficient torque to cope with the BLDC wheel hub motors.

Figure 5 also reveals that when superimposing the maximum torque and power versus speed curves onto the dynamometer envelope. It is clearly seen that the dynamometer can only measure the torque and power curves of the BLDC wheel hub motors when the

performance curves are inside the envelope of the alternator.

For the Lunyee TX48 48V – 1000W BLDC wheel hub motor, nearly the first half of the performance curves at the transmission ratio of 4 are outside the alternator characteristics. Hence, the dynamometer only has the ability to create the resisting torque at the alternator speed range from 2000 to 4600 rpm for this case. For performance curves at the remaining two transmission ratios, the dynamometer can only measure the later part of the performance curve. There is only a petite section of performance curves that cannot be investigated in these cases, which is approximately at the alternator speed range from 350 to 1400 rpm for the transmission ratio of 12 and between 900 and 1200 rpm for the transmission ratio 30.

Meanwhile, the Golden Motor MP4 – 24V – 200W BLDC wheel hub motor's performance curves at a transmission ratio 4 are entirely outward of the dynamometer envelope and thus cannot be measured in this case. On the other hand, in the case of the transmission ratio of 30, the dynamometer is completely capable of covering the whole performance curve. This means that all the torque and power versus speed curves, in this case, can be investigated. Finally, in the remaining case, there is just a tiny fraction of the performance curves in the alternator speed range between 800 and 1200 rpm that the dynamometer can not cover.

3.4 Electric load system

In this design, the electrical load must ensure that it can handle the maximum power output of the alternator, which is 1.1kW at 12VDC. As mentioned in section 2.3, the headlight bulbs are selected for the electrical load. Therefore, the authors decided to use an OSRAM H4 halogen bulb with a power rating of 100/90W and a voltage of 12VDC. Figure 6 presents the wiring diagram of the electrical load system. By utilizing 12 bulbs connected in parallel, the total load capacity of the electrical load amounts to 1.2kW. A MOSFET, also known as a proportional control switch, is used to adjust the power consumption of the bulbs and create various load levels. By varying the current passing through the bulbs at a constant voltage of 12VDC, the load power can be adjusted accordingly through the control system (more detailed in Section 3.5).

Figure 7 presents the construction of the electrical load, including insulated shells, light bulbs, and cooling fans. The horizontal distance between the bulbs is 127.5 mm, while the vertical distance is 150 mm. These bulbs are housed within an insulated shell made of mica, which is intended to protect the bulbs from external damage and minimize the impact of high temperatures on nearby users. The shell is located on the right side of the dynamometer frame and is attached to the frame with bolts and nuts. A rubber gasket is placed between the mica shell and the frame to prevent damage to the shell. To improve convenience and simplify the installation of our load system, the authors have designed a custom socket holder for the OSRAM H4 halogen bulbs. This holder securely positions the bulbs, ensuring correct alignment for optimal load generation. Additionally, four cooling fans will be installed vertically on the right side of the enclosure to ensure the operational stability of the bulbs. The specifications for the fan type are provided in Table 1.

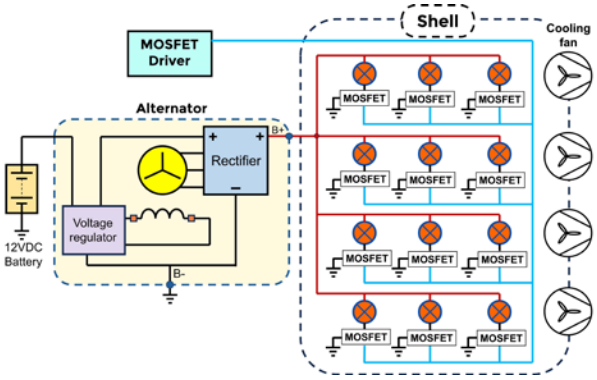

Figure 6. Schematic diagram of electrical load system.

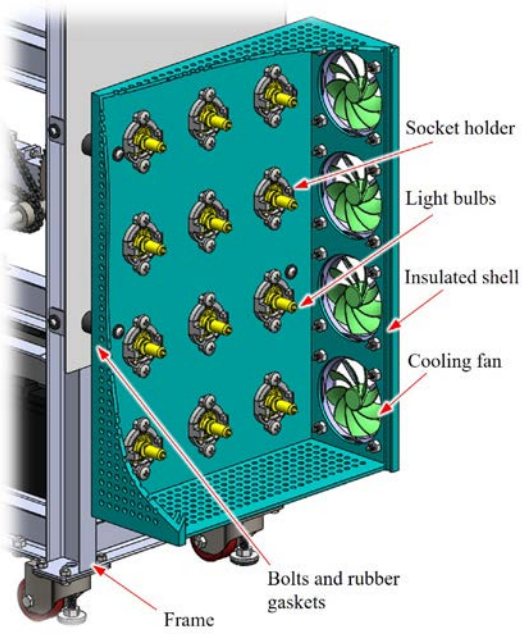

Figure 7. Structure of the electrical load system.

Table 1. Properties of the cooling fan

Parameter	Value
Rated voltage (V)	Single phase 220
Rated current (A)	0.45
Rated speed (rpm)	2000
Air flow rate (CFM)	100

3.5 Controller

3.5.1 Scheme of the controller

The controller must ensure the collection of torque va–lues corresponding to each speed at various load levels. As shown in Figure 8, the controller includes essential input signals, specifically the frequency from the alter–nator AC voltage for calculating the motor speed, as well as a torque sensor for measuring the motor torque. Additionally, it incorporates a unit that monitors the input power supplied to the electric motor, which includes voltage and current measurements to calculate the efficiency of the motor on the dynamometer test bench.

The output of the controller will be the throttle signal applied to the BLDC driver corresponding to different load levels and the power consumption of the electrical load (headlight bulbs), which creates a resistive load on the motor. This setup enables the acquisition of torque and speed values at each load condition.

The processing unit will consist of a microcontroller and a signal conditioning circuit, specifically a zero-crossing detection circuit, to convert the sine wave voltage signal from the alternator into a square wave. Using the input capture feature of the microcontroller, the frequency or speed of the alternator rotor will be determined. The signals from the power measurement module for the electric motor will be measured using the ADC peripheral. For the output, the power stage circuit includes a Low-pass filter and Buffer circuit that ensures the PWM signal from the microcontroller is converted to analog, providing the throttle signal to the BLDC driver for effective speed control. Additionally, MOSFETs are utilized in conjunction with a FET drive, which is also controlled by the PWM output from the microcontroller, to adjust the electric power consumption of the headlight bulbs, thereby creating a resistance against the motor rotation, as previously mentioned.

Furthermore, the torque sensor signal cannot be determined directly; instead, it requires a torque trans–mitter to obtain a more accurate torque value. This device communicates using the RS-485 standard. Thro–ugh RS-485 transceiver interface ICs, the micro–controller can connect to this module and receive torque value from the sensor.

The hardware was selected to match each other and ensure control of the dynamometer in all measuring cases. The specifications of the hardware are presented in Table 2.

Table 2. Hardware specifications

Device	Specific parameter	Value
Regulator - LM2576 Adj	Maximum input voltage	45 V
	Output voltage	Adjustable output voltage (9 V)
Regulator - LM7805C	Input voltage	7 to 25 V
	Output voltage	5 V
Microcontroller - STM8S207C8T6	Supply management	2.95 to 5.5 V operating voltage
	ADC	10-bit, 16 channels
	Clock	External clock 24 MHz
	Timer	2x16-bit with 2+3 CAPCOM channels (IC, OC or PWM)
	UART	3x programable UARTs
Current sensor - ACS756-050	Supply voltage	3.0 to 5.0 V
	Primary Sampled Current	-50 to 50 A
Torque sensor - DYJN-101	Torque capacity	50 Nm
	Working power	5 to 10 V
Torque transmitter - D810	Power supply voltage	15 to 30 V (24 V recommended)
	Communication	RS485, Modbus-RTU
RS485 transceiver - SP485	Power supply voltage	4.75 to 5.25 V
	Maximum data rate	5 Mbps
USB to TTL IC - FT232	Operating supply voltage	4.0 to 5.25 V
	I/O voltage	1.8 to 5.0 V
	USB speed	Full speed 2.0 (12Mbps)
	Data transfer rate	3 Mbaud
Filter + Buffer - LM358N	Power supply voltage	3.0 to 32 V
FET driver - TLP250	Power supply voltage	10 to 35 V
	Operating frequency	25 kHz
MOSFET - IRF3205	Drain to source breakdown voltage	55 V
	Continuous drain current	110 A
	Gate threshold voltage	4 V

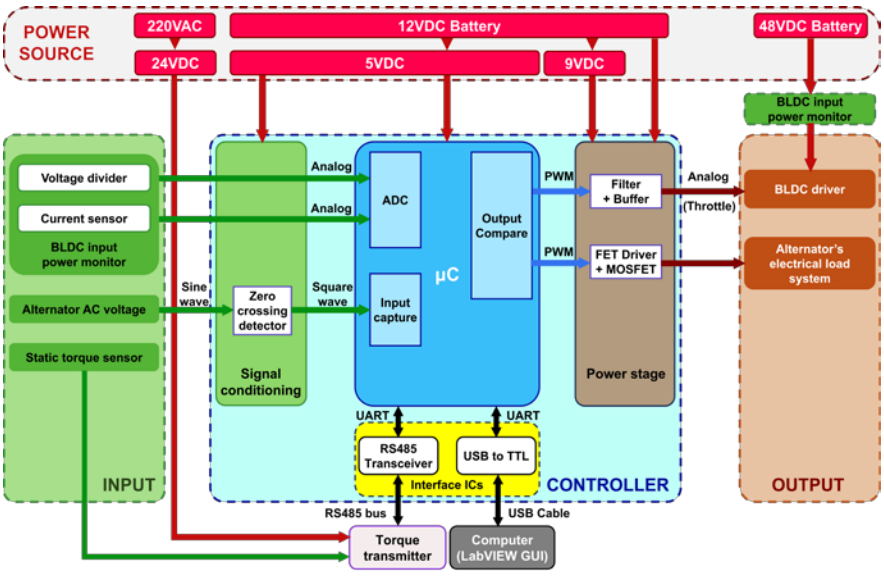

Figure 8. Scheme diagram of the controller.

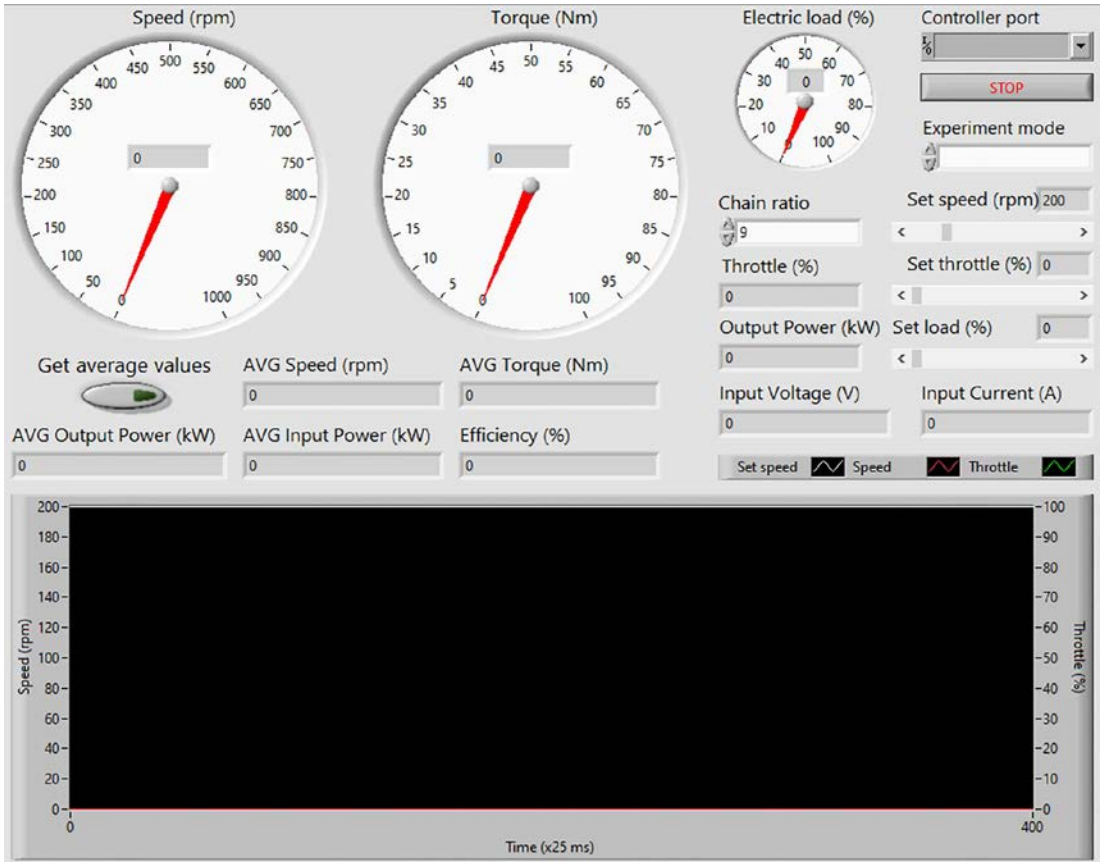

Figure 9. The front panel of LabVIEW GUI.

3.5.2 Graphic user interface (GUI)

The GUI is designed to collect and monitor dynamo–meter operating parameters, as well as set the mode and operating parameters for the system, which is shown in Figure 9.

The displayed parameters include the alternator rotor speed – combined with the ratio of the chain drive under certain operating conditions, which is manually entered into the interface to calculate the electric motor speed, electric motor torque, voltage, and current supplied to the BLDC driver, thereby calculating the motor output mechanical power and the input electrical power supplied to the driver, calculating the overall efficiency of the motor and the driver.

The speed and torque of the motor are displayed by an analog gauge and a digital display in the center of the gauge. In addition, the motor speed is also displayed on a graph over time so that the user can determine that the system is operating stably before taking an average operating parameter value to make the experimental results.

Accordingly, when selecting to operate in speed mode, the user interacts with the controller to operate the dynamometer through two variables: set speed and load. After getting these set values, the controller calculates the set throttle value and simulates the throttle signal input to the BLDC driver to ensure the desired speed is established.

Meanwhile, when the operating mode is selected as torque mode, the two manually set variables are throttle and load. The controller simulates the throttle signal input to the BLDC driver.

The collected parameters are sent from the microcontroller to the controller at regular intervals, while the set data values are only sent back to the controller when the user sets a new operating point. The average values recording operation is performed when the user determines that the engine speed graph is stable over time. The average values displayed include speed, torque, voltage, and current; along with input power, output power, and overall efficiency of the motor's driver and BLDC.

3.6 Chain drive system

As mentioned in Section 3.3, it is apparent that the operating speed range difference between the alternator and both of the BLDC wheel hub motors is significantly large. Therefore, the chain drive's overall transmission ratio is selected at 4, 12, and 30. Furthermore, it is designed to change the overall transmission ratio flexibly.

Table 3. Transmission ratio distribution at three-stage drive

	BLDC to Shaft I	Shaft I to Shaft II	Shaft II to Alternator
Transmission ratio	$i_{\mathrm{I}} = 1/4$	$i_{\mathrm{II}} = 1/3$	$i_{\mathrm{III}} = 1/2.5$

Table 4. Transmission ratio distribution at two-stage drive

	BLDC to Shaft I	Shaft I to Alternator
Transmission ratio	$i_{\mathrm{I}} = 1/4$	$i_{\mathrm{II}} = 1/3$

The overall transmission ratio of 1/30 and 1/12 is too high because the overall transmission ratio of the single-stage chain drive can not exceed 1/5 [21]. The overall transmission ratio of 1/30 and 1/12 is too high because

the overall transmission ratio of the single-stage chain drive can not exceed 1/5 [21]. Thus, a three-stage drive and a two-stage drive for the overall transmission ratio of 1/30 and 1/12, correspondingly, are chosen. The transmission ratio distribution at three-stage drive and two-stage drive are shown in Table 3 and Table 4, respectively.

3.6.1 Selecting the number of sprocket teeth and chain type

Table 5. The number of sprocket teeth corresponds at different stages of each overall transmission ratio

Stage	Symbol	Number of sprocket teeth	
		1/30 transmission ratio	1/12 transmission ratio
1st stage	N_1	60	
	N_2	15	
2nd stage	N_3	45	
	N_4	15	
3rd stage	N_5	40	-
	N_6	16	-

To facilitate changing the transmission ratio during operation, the first two transmission ratios of the two-stage and three-stage drive will be the same in terms of the number of drive and driven sprocket teeth, which are initially selected at N_1 = 60 teeth and N_2 =15 teeth for the 1st stage, and N_3 = 45 and N_4 = 15 teeth for the 2nd stage. At the same time, the 3rd stage of the 1/30 transmission ratio is provisionally selected at N_5 = 40 teeth for the drive sprocket and N_6 = 16 teeth for the driven sprocket. The parameters of the chain drive system are shown in Table 5.

Re-checking the overall transmission ratio by the following formulas [21]:

$$i_{30} = \frac{N_2}{N_1} \times \frac{N_4}{N_3} \times \frac{N_6}{N_5} \tag{1}$$

$$i_{12} = \frac{N_2}{N_1} \times \frac{N_4}{N_3} \tag{2}$$

where i_{30} and i_{12} are the overall transmission ratio at three-stage drive and two-stage drive, respectively.

Substituting the value of number of teeth in Table 4 above into equation (3) and (4). As a result, the overall speed ratios of two-stage and three-stage drives still remain the same, which are 1/30 and 1/12, respectively.

The tooth factor for each stage is estimated:

$$K_2 = 19/N_i \tag{3}$$

where K_2 is the tooth factor, N_i is the number of ith-driven sprocket teeth

Substituting the value of the smallest number of driven sprocket teeth (15 teeth) into equation (5), we get the result of the tooth coefficient K_2, which is 1.266.

Additionally, This chain drive mechanism is classified as smooth running with a single-row chain. Thus, the application factor K_1 is selected at 1 for the whole stage of each overall transmission ratio. Therefore, the corrected power transmission at different stages of each overall transmission ratio is determined as follows [21]:

$$P_c = P_e \times K_1 \times K_2 = 1.27 \text{ (kW)} \tag{4}$$

where P_c is the corrected power kW), and P_e = 1 kW is the power of the BLDC motor.

Searching the BS chain drives rating chart [21] for a combination of rotational speed at different stages of each overall transmission ratio and 1.27 kW of corrected power transmission provides a 9.525 mm pitch simple BS chain, which is suitable for the dynamometer's chain drive system.

3.6.2 Calculating the center distance and chain length

The initial center distance is calculated [21]:

$$a_i = (30 \div 50)\, p = 288.8 \div 476.3 \text{ (mm)} \tag{5}$$

where a_i is the center distance of ith stage (mm), p = 9.525 mm is the chain pitch.

Consequently, the center distance at different stages of each overall transmission ratio is provisionally selected following the initial result above to ensure the chain drive's stability and achieve the compact size of the whole system. The initial results are summarized in Table 6.

Table 6. The initial center distance at different stages of each overall transmission ratio

Parameters	Symbol	Unit	Value
1st stage center distance	a_{I_30}, a_{I_12}	mm	320
2nd stage center distance	a_{II_30}, a_{II_12}	mm	460
3rd stage center distance	a_{III_30}	mm	410

As the three-stage drive and two-stage drive use the same sprockets with the same transmission ratio at the first two stages, the center distance of the first two stages of each overall transmission ratio is equal.

The number of pitches is estimated by the following formula [21]:

$$L_i = \frac{N_i + N_j}{2} + \frac{2a_i}{p} + \left(\frac{N_i - N_j}{2\pi}\right)^2 \frac{p}{a} \tag{6}$$

where L_i is the chain pitch of ith stage (pitches), N_i and N_j are the number of ith drive sprocket teeth, and the number of jth driven sprocket teeth, respectively.

The results of the number of pitches at different stages of each overall transmission are summarized in Table. 7. Note that all the values in this Table are rounded up to the nearest even integer.

Table 7. The number of pitches at different stages of each overall transmission ratio.

Parameters	Symbol	Unit	Value
The number of pitches of 1st stage chain	L_{I_30}, L_{I_12}	Pitches	108
The number of pitches of 2nd stage chain	L_{II_30}, L_{II_12}	Pitches	128
The number of pitches of 3rd stage chain	L_{III_30}	Pitches	116

The actual center distance is determined as below [21]:

$$a_i = \frac{p}{8}\left[2L_i - N_i - N_j + \sqrt{\left(2L_i - N_i - N_j\right)^2 - \frac{\pi}{3.88}\left(N_i - N_j\right)^2}\right] \quad (7)$$

Substituting the result of the number of pitches in Table 7 into equation (9). Finally, the actual center distance at different stages of each overall transmission is illustrated in Table 8.

Table 8. Actual center distance at different stages of each overall transmission ratio

Parameters	Symbol	Unit	Value
1st stage center distance	a_{I_30}, a_{I_12}	Mm	328
2nd stage center distance	a_{II_30}, a_{II_12}	Mm	463
3rd stage center distance	a_{III_30}	Mm	416

Calculating the intermediate shaft strength

Figure 10 illustrates the broken-out section of the intermediate shaft I. The intermediate shaft provides positions for chain sprockets to place and also transmits the power from the BLDC motor to the alternator. Therefore, it must withstand the combinations of torsional and bending moments while operating, which are created by the chain drive and the weight of components assembled on it.

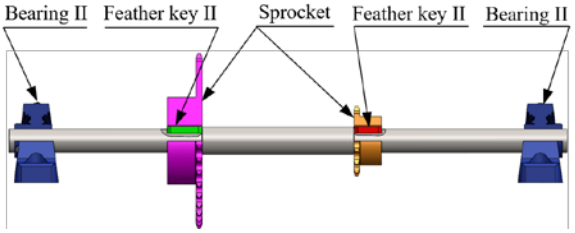

Figure 10. Broken out the section of the intermediate shaft I.

In this section, the strength of the intermediate shaft is only calculated and verified on the intermediate shaft I at the low operating speed range of the Lunyee TX48 – 48V BLDC wheel hub motor due to the highest torque and tangential force appearing in this mode. The shaft's material is AISI 1045 steel, and the safety factor (fs = 3) is used to calculate and simulate shaft strength. Furthermore, the specifications of the TX48 BLDC motor, including rotational speed and power, are used to determine the intermediate shaft's strength in this whole section.

Besides, these intermediate shafts are 400 mm in length and are designed to have stepped with a larger shaft diameter at the center with the value of 20 mm, enhancing strength and preventing the axial movement of two sprockets on each shaft. On the other hand, the diameter of both shaft ends is selected at 17 mm, which corresponds to the sprocket hub's diameter.

The average velocity of the chain is calculated by the formula below [22]:

$$v_I = \left(N_1 p n_e\right)/60000 = 0.3 \text{ (m/s)} \quad (8)$$

$$v_{II} = \left(N_3 p n_I\right)/60000 = 0.9 \text{ (m/s)} \quad (9)$$

where v_I and v_{II} is the chain's average velocity of 1st stage and 2nd stage drive (m/s), respectively. N_1 = 60 teeth and N_3 = 45 teeth are the 1st stage and 2nd stage drive sprocket's number of teeth, respectively. n_e = 29.9 rpm and n_I = 119.6 rpm are the rotational speeds of the BLDC motor and the intermediate shaft I, correspondingly.

The tangential force acting on chain or shaft load is obtained as follows [22]:

$$F_{t\_I} = \left(1000 P_{e.min} \times 10^{-3}\right)/v_I = 379 \text{ (N)} \quad (10)$$

$$F_{t\_II} = \left(1000 \times P_{e.min} \times 10^{-3}\right)/v_{II} = 120 \text{ (N)} \quad (11)$$

where F_{t_I} and F_{t_II} are the tangential force acting on the chain of 1st and 2nd stage drive (N), respectively. $P_{e.min}$ = 113.7 W is the TX 48 BLDC motor power at maximum torque [19].

The tangential force F_{t2L} is divided into x and y components because the intermediate shafts I and II are arranged with the inclined angle (α) of 45 degrees. Hence, these two components are obtained by the following equations [22]:

$$F_{x\_II} = F_{t\_II} \sin\alpha = 84.9 \text{ (N)} \quad (12)$$

$$F_{y\_II} = F_{t\_II} \cos\alpha = 84.9 \text{ (N)} \quad (13)$$

where F_{x_II} and F_{y_II} are the x and y components of tangential force F_{tII} (N), respectively.

The maximum torque T exerted on the intermediate shaft I at 29.9 rpm is 36.3 Nm [19].

The strength of intermediate shaft I is simulated via Solidwork Simulation. All the calculated tangential force and torque above are entered into this software, which is shown in Figure 11.

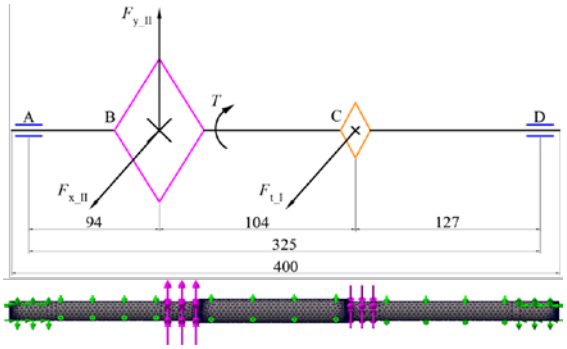

Figure 11. Forces and torque are exerted on the intermediate shaft.

3.6.3 Calculating the intermediate shaft strength, feather keys, and bearings

The reaction forces on bearing locations (in sections A and D) are presented in Figure 12. It is clearly seen that the reaction forces on both sections are almost similar because the tangential forces applied on the shaft are far from bearing locations.

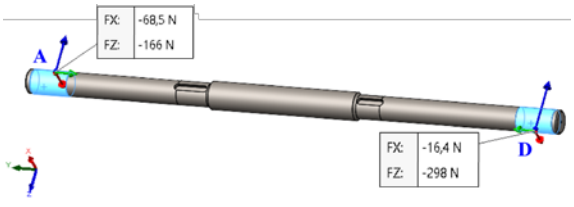

Figure 12. Reaction forces on bearing locations.

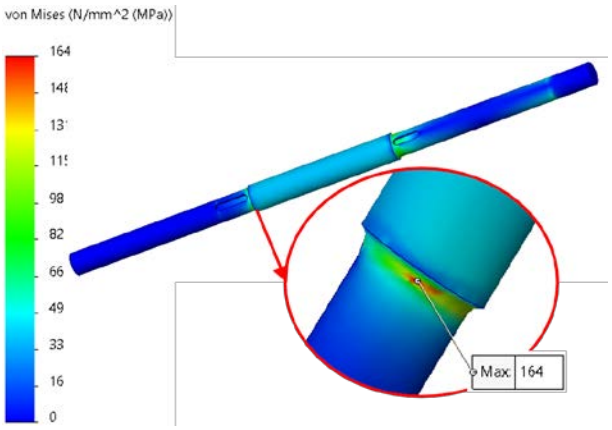

Figure 13. Stress diagram of the intermediate shaft I

Figure 13 depicts the stress diagram of the inter–mediate shaft I. The results illustrate that the highest stress occurs at the shaft's stepped location, where the drive sprocket of 2nd stage drive is located. It has the value σ_{max} = 164 MPa and is significantly lower than the yield strength of AISI 1045 steel ([σ] = 176.7 MPa with the safety factor (*fs*) of 3). As a result, all intermediate shafts of the chain drive system ensure strength.

Calculating the feather keys

The intermediate shafts are designed to have two feather keys on them, which is illustrated in Figure 9. These keys connect the intermediate shafts with the chain sprocket to transmit torque from the shaft to the chain sprocket's hubs, and they also prevent the rotational motion between the shaft and chain sprocket. Conse–quently, these feather keys are subjected to shear and compressive stresses created by the BLDC motor torque.

The feather key's material and safety factor (*sf*) is the same as the intermediate shaft. Following the maximum shear stress theory of failure [22], the shearing stress is halved of the material yield strength. Hence, the allowable shear stress with safety factor *sf* = 3 is obtained as below [22]:

$$\tau = 0.5S_y / sf = 88.3 \text{ (MPa)} \tag{14}$$

where τ is the allowable shear stress, and S_y = 530 MPa is the AISI 1045 steel's yield strength [23].

Based on the feather key selection guide [22], the width and height of the feather key are one-fourth of the shaft diameter. Thus,

$$b = h = d/4 = 4.3 \text{ (mm)} \tag{15}$$

where *b*, *h* are the width and height of the feather key (mm), correspondingly. *d* = 17 mm is the diameter of the intermediate shaft at feather key locations.

Finally, the feather key length is determined using this equation [22]:

$$l = \left(2T \times 10^3\right) \Big/ \left(\tau db\right) = 11.2 \text{ (mm)} \tag{16}$$

Searching the feather key standard dimensions and according to the chain sprocket's hub dimensions, the dimensions of the key are selected at 5 × 5 × 20 mm and 5 × 5 × 25 mm.

Calculating the bearing

Using the reaction forces acting on sections A and D of the intermediate shaft, as depicted in Figure 12, the critical section of the bearing location is section D. It is assumed to neglect the axial load in the calculation process since its value is too small. Thus, the bearing is subjected to pure radial forces, and its value in this bearing location is determined as follows [22]:

$$F_{rD} = \sqrt{R_{Cx}^2 + R_{Cy}^2} = 298.5 \text{ (N)} \tag{17}$$

where F_{rD} is the radial force at section D, R_{Cx} = 16.4 N, and R_{Cz} = 298 N are the reaction forces on the vertical and horizontal plane, respectively.

Then, the equivalent dynamic load at section D is obtained by using the following formula [22]:

$$P_{bD} = XF_{rD} = 298.5 \text{ (N)} \tag{18}$$

where P_{bD} is the equivalent dynamic load at section D (N), and X = 1 is the radial loading factor.

The million revolutions of the bearing or bearing life are determined below [22]:

$$L_{10} = 60 n_{max} L_{10h} = 1440 \cdot 10^6 \text{ (rev.)} \tag{19}$$

where L_{10} is the bearing life (revolutions), $n_{2L.max}$ = 3000 rpm is the approximately maximum rotational speed of 2nd stage drive, and L_{10h} = 8000 hours is the expected life of the bearing.

The dynamic load capacity is obtained by the following equation [22]:

$$C = P_{bD} \left(L_{10}\right)^{1/3} = 3370.8 \text{ (N)} \tag{20}$$

where *C* is the dynamic load capacity (N).

As a result, the SKF SY 17 TF pillow block ball bearing is chosen for the chain drive system with the following technical specifications [24]: the maximum rotational speed of 9500 rpm, basic dynamic load rating *C*, and basic static load rating C_o are 9560 N and 4750 N in the order given.

3.7 Dynamometer frame

Figure 14 illustrates the simulation model of the dynamometer frame. U-channel of 62×35×33 mm and 50×30×2.6 mm rectangular tube followed by ASTM A36 steel standards are chosen to manufacture the dynamometer frame. The frame consists of four levels: the bottom level will be used to contain the battery, while the second and third levels will be used to attach the BLDC motor, chain drive system, alternator, and mounting devices. Finally, the top level provides a place for arranging computers. In addition, the controller and electric load system will be installed on the side of the frame. All steel bars and equipment mounting slots are laser cut and then welded together, creating the frame's overall dimensions of 982×457×1045 mm and weighing about 36.5 kg, achieving aesthetic and compactness in size.

While operating, the frame withstands dynamic load, which is created by the vibration of the chain drive system and static load from all components assembled on

it. Figure 14 also depicts the load distribution and mes–hing model of the dynamometer frame. The mesh type is curvature-based, with the highest element size of 17 mm.

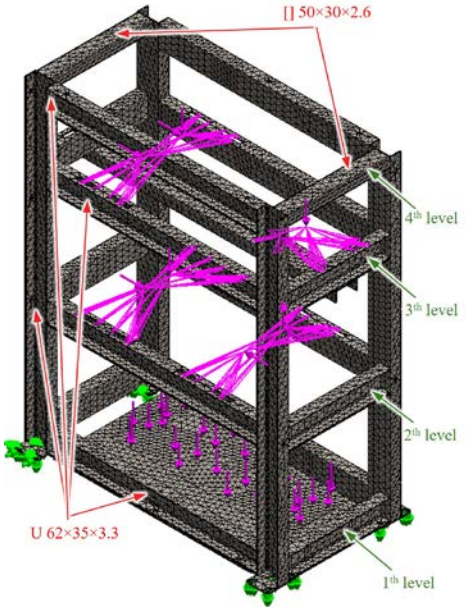

Figure 14. Structure and simulation model of frame.

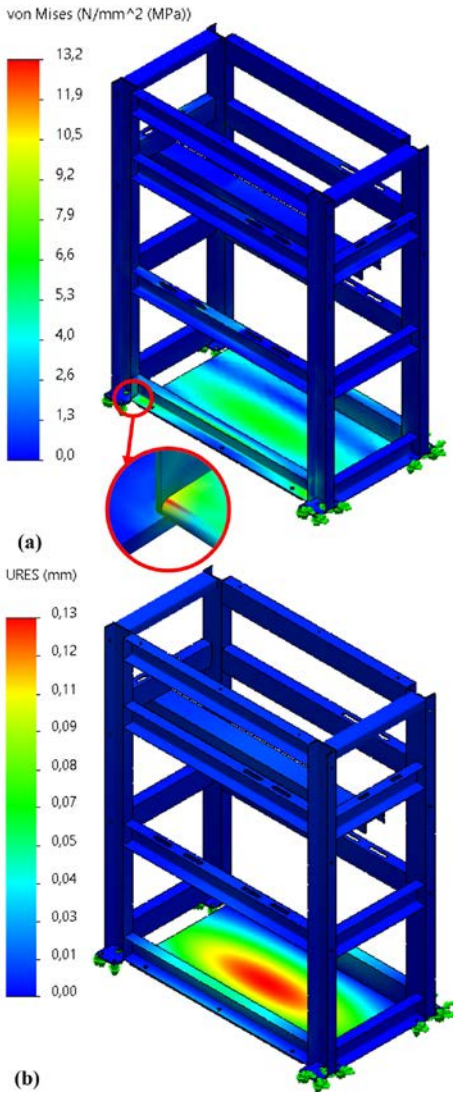

Figure 15. The dynamometer frame's simulation results (a) Stress diagram and (b) Displacement diagram.

The results of stress and displacement are illustrated in Figure 15. It is clearly seen that the location of maximum stress appears on the edge of the long horizontal bar at the bottom floor of the frame with the value of approximately σ_{max} = 13.2 MPa, whereas 0.13 mm is the most considerable displacement value, located in the middle of the bottom floor. Hence, these results are reasonable and satisfy the strength condition because the maximum stress is below the yield strength of the material (245 MPa).

4. GENERAL LAYOUT AND MANUFACTURING MODEL

The 3-dimensional general layout drawings of the dynamometer used for small electric motors with 2-stage and 3-stage chain drives are shown in Figure 16 and Figure 17, respectively. BLDC motor with the static torque sensor attached to its shaft will be arranged on the frame's 2nd level, as well as the intermediate shaft I and its components. The 3-stage drive arrangement differs from the 2-stage drive arrangement in adding the intermediate shaft II and its components, leading to the alternator's installation position being in the opposite direction. Besides, other systems are organized simi–larly, which means they are not different. The battery is arranged at the bottom level, while the controller and electric load system are installed on the side of the frame. This arrangement will give the flexibility to change the overall speed ratio of the system and achieve the compactness of the entire system with the overall length, width, and height of 993 × 467 × 1054 mm.

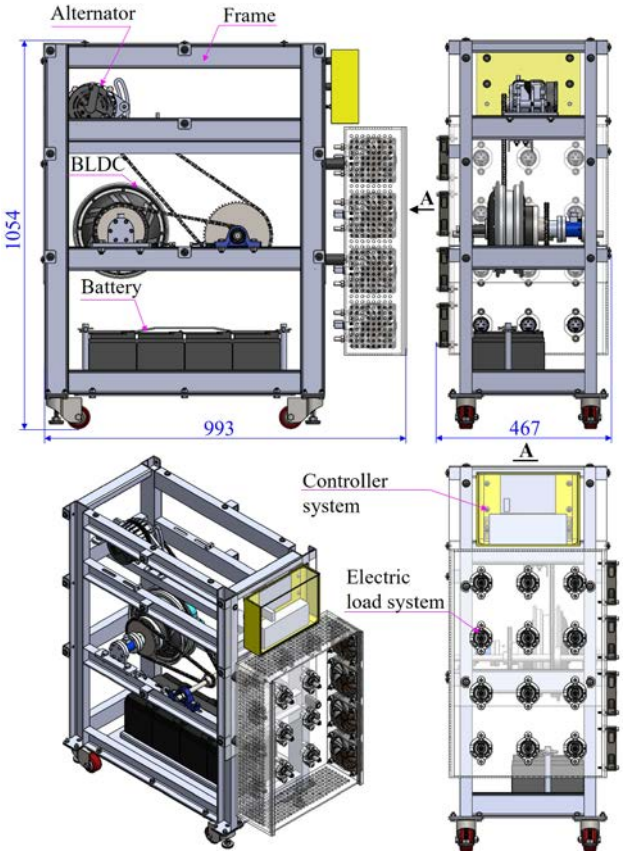

Figure 16. The 3D general layout drawing of the dynamometer with a 2-stage drive.

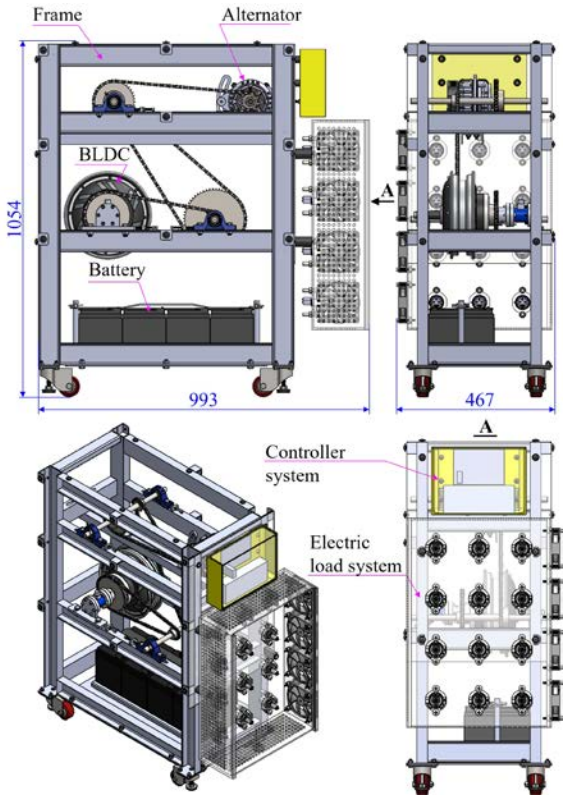

Figure 17.The 3D general layout drawing of the dynamometer with a 3-stage drive.

Figure 18 illustrates the actual model of the dyna–mometer used for small electric motors with a 3-stage drive and describes a more detailed view of each system in the dynamometer. The alternator is assembled on the 3rd level of the frame by the mounting devices, which also tension the chain. To directly measure torque, one end of the BLDC motor shaft is attached to the static torque sensor via a coupling, and this cluster is placed on the frame by a mounting device. The other end of the BLDC motor is held by a pillow block ball bearing. Furthermore, the controller and the electric load system are connected to the side of the dynamometer's frame by bolt joints.

5. CONCLUSIONS

In this paper, the dynamometer for small electric motors has been designed and implemented. All sub-systems, including the chain drive system, frame, control system, user interface, and electric load system, have been developed and combined to create a complete system that can investigate various performance characteristics of small electric motors.

An automobile alternator was selected based on the requirements for investigating the characteristics of small electric motors. Then, a chain drive with a flexible transmission ratio was designed to connect the electric motor and the alternator. At the same time, an appropriate electrical load system that can consume all of the alternator's output power was designed. The drivetrain was deeply analyzed and designed to assess the electric motor's speed characteristics over its entire operating range. In particular, a three-stage chain drive was designed with transmission ratios of 1/4, 1/3, and 1/2.5.

The controller was designed to control the whole dynamometer and collect the necessary data to build the characteristics of the electric motor, including speed, output torque, output power, input current, and input voltage. In particular, the controller can continuously and automatically adjust the electric load level to determine the motor's part-load and full-load characteristics under both constant load level and throttle settings. In addition, the graphic user interface is built on the computer to help communicate with the controller quickly and easily.

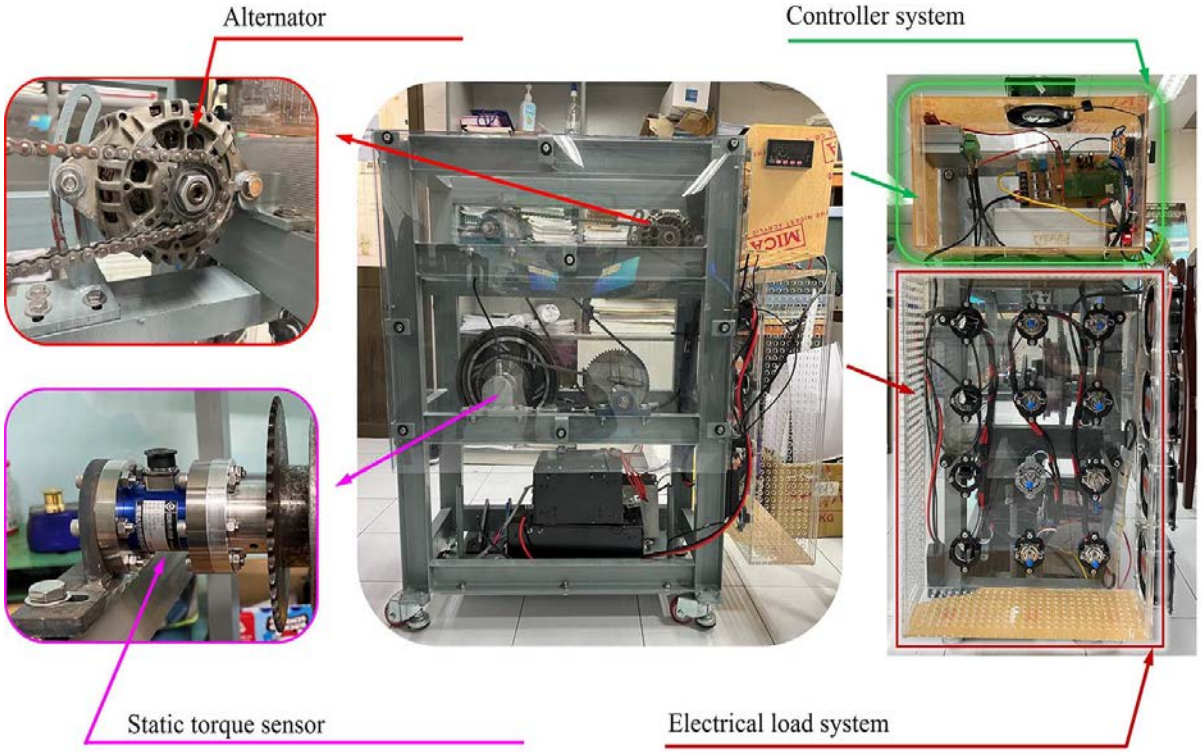

Figure 18. The actual model of the dynamometer system with a 3-stage drive.

Overall, the studied dynamometer is compact, easy to manufacture with available, affordable materials, and easy to operate and maintain. The flexibility of the chain drive system's transmission ratio and the comprehensive algorithm control of the controller allows the dynamometer to experiment with various performance characteristics of different electric motors. This design can be extended to investigate various electric motors with power within 3000W.

This dynamometer is a powerful tool for researching electric motor characteristics, which contributes to developing control algorithms and enhancing electric motorbikes' performance and working range. The proposed design method can be applied to create dynamometers for popular electric motorbike motors with higher power of up to 10 kW. It also plays a vital role in meeting the growing demand for electric vehicle research in developing countries (e.g., Vietnam, Indonesia, Laos, etc.) in the context of the current dynamometer systems on the market, which are costly.

ACKNOWLEDGMENT

We acknowledge Ho Chi Minh City University of Tec–hnology (HCMUT), Vietnam National University Ho Chi Minh City (VNU-HCM) for supporting this study.

REFERENCES

[1] Ehsani, M., Yimin. G., Gay, S.: Characterization of electric motor drives for traction applications, in: *IECON'03 29th Annual Conference of the IEEE Industrial Electronics Society (IEEE Cat No03CH37468)*, 2003, Roanoke, pp. 891–896.

[2] Hashemnia, N., Asaei, B.: Comparative study of using different electric motors in the electric vehicles, in: *2008 18th International Conference on Electrical Machines*, 2008, Algarve, Paper 1257.

[3] Jouanne, A. V., Adegbohun, J., Collin, R., Stephens, M., Thayil, B., Li, C., et al.: Electric Vehicle (EV) Chassis Dynamometer Testing, in: *2020 IEEE Energy Conversion Congress and Exposition (ECCE)*, 2020, Detroit, pp. 897–904.

[4] Alibek, I., Bakhyt, A., Troha, S., Marković, K., Vrcan, Ž.: Efficiency-based methodology for the selection of electric motors for mini-tractor propulsion, FME Trans, Vol. 52, pp. 360–370, 2024.

[5] Milićević, S., Blagojević, I., Muždeka, S.: Advanced rule-based energy management for better fuel economy of hybrid electric tracked vehicle, FME Trans, Vol. 49, pp. 711–718, 2021.

[6] Sun, Y., Wang, Y., Zhu, R., Geng, R., Zhang, J., Fan, D., et al.: Development of test bed of hybrid electric vehicle based on chassis dynamometer, IOP Conf. Ser. Mater. Sci. Eng, Vol. 452, p. 042112, 2018.

[7] He, P., Dong, Z. R., Han, C. W., Hu, S. H.: Design and test development of a comprehensive performance test bench for electric wheel, Appl. Mech. Mater, Vol. 644-650, pp. 817–22, 2014.

[8] Hassan, M. H., Sapee, S., Nafiz, D. M., Yusop, A. F., Basrawi, M. F., Rasid, A. H.: Chassis dynamo–meter for electric two wheelers, MATEC Web of Conferences. Vol . 225, p. 03016, 2018.

[9] Su, D. T., Shiao, Y. S., Yang, J. L.: Design and Implementation of a Chassis Dynamometer for Testing Battery-Powered Motorcycles. WSEAS Trans. Circuits Syst, Vol. 7, pp. 879-889, 2008.

[10] Firmansyah, A. I., Supriatna, N. K., Gunawan, Y., Setiadanu, G. T., Slamet: Performance Testing of Electric Motorcycle Conversion, in: 7*th International Conference on Electric Vehicular Technology, ICEVT 2022 – Proceeding*, 2022, Seminyak-Kerobokan Bali, pp. 165–168.

[11] Kumar, M. S., Revankar, S. T.: Development scheme and key technology of an electric vehicle: An overview, Renew. Sustain. Energy Rev, Vol. 70, pp. 1266–1285, 2017.

[12] Dukalski, P., Mikoś, J., Krok, R.: Analysis of the Simulation of the Operation of a Wheel Hub Motor Mounted in a Hybrid Drive of a Delivery Vehicle, Energies, Vol. 15, p. 8323, 2022.

[13] Cao, Z., Mahmoudi, A., Kahourzade, S., Soong, W. L.: An Overview of Electric Motors for Electric Vehicles, *31st Australasian Universities Power En–gineering Conference (AUPEC)*, 2021, Perth, pp. 1–6.

[14] Racewicz, S., Kazimierczuk, P., Kolator, B., Olszewski, A.: Use of 3 kW BLDC motor for light two-wheeled electric vehicle construction, IOP Conf. Ser. Mater. Sci. Eng. Vol. 421, p. 042067, 2018.

[15] Kolator, B., Racewicz, S., Olszewski, A.: Bench tests results of the traction parameters of the light two-wheeled electric vehicle, IOP Conf. Ser. Mater. Sci. Eng, Vol. 421, p. 022015, 2018.

[16] Kang, D. K., Kim, M. S.: Determination of the road load on electric two-wheelers using the torque-current relationship of the drive motor, J. Mech. Sci. Technol, Vol. 30, pp. 4023-4029, 2016.

[17] Martyr, A. J., Plint, M. A.: *Engine Testing Theory and Practice, 3rd edition*, Oxford, Butterworth-Heinemann, 2007.

[18] Golden Motor. MP4-24V-15A50T Test report, 2011, Available from: https://www.goldenmotor.com/frame22-hub.htm, Accessed: Aug. 10th 2024.

[19] Lunyee Industries. TX48-48V-1000W Hub motor Conversion kit, 2024, Available from: https://www.lunyee.com/products/350-1000w-36-48v-30-65km-per-hour-hub-motor-conversion-kit.html, Accessed: Aug. 8th 2024.

[20] Remy, D.: Electrical Specifications and Selection Guide: Starters and Alternators, 2006, Available from: https://www.delcoremy.com/find-a-part/product-details/1101307/12si-new-alternator, Accessed: Aug. 8th 2024.

[21] Childs, P. R. N.: *Mechanical Design Engineering Handbook, 2nd ed*, Oxford, Butterworth-Heine–mann, 2019.

[22] Bhandari, V. B.: *Design of machine elements. 3rd ed*, Tata McGraw-Hill, 2010.

[23] MW Components. Carbon Steel Grade 1045 Fact Sheet, 2024, Available from: https://www.mwcomponents.com/uploads/Resource-Center/Elgin-Material-Sheets/Carbon-Steel-Grade-1045-Fact-Sheet_Elgin-Website.pdf, Accessed: Jul. 26th 2024.

[24] SKF. SY 17 TF, 2024, Available from: https://www.skf.com/us/products/mounted-bearings/ball-bearing-units/pillow-block-ball-bearing-units/productid-SY%2017%20TF, Accessed: Aug. 6th 2024.

NOMENCLATURE

a	Center distance (mm)
b	Width of the feather key (mm)
C	Dynamic load capacity (N)
C_o	Basic static load rating
d	Diameter of the intermediate shaft at feather key locations (mm)
F_{t_I}	Tangential force acting on the chain of 1st stage drive (N)
F_{t_II}	Tangential force acting on the chain of 2nd stage drive (N)
F_{x_II}	x components of tangential force F_{t_II} (N)
F_{y_II}	y components of tangential force F_{t_II} (N)
F_{rD}	Radial force at section D (N)
h	Height of the feather key (mm)
i	Transmission ratio
K_2	Tooth factor
K_1	Application factor
L	Number of chain pitches
L_{10}	Bearing life, revolutions
L_{10h}	Expected life of the bearing (hours)
l	Length of the feather key (mm)
N	Number of sprocket teeth
n_e	Rotational speed of BLDC motor (rpm)
n_I	Rotational speed of intermediate shaft I (rpm)
$n_{2L.max}$	Approximately maximum rotational speed of 2nd stage drive (rpm)
P	BLDC motor power (kW)
P_c	Corrected power (kW)
p	Chain pitch (mm)
P_{bD}	Equivalent dynamic load at section D (N)
$P_{e.min}$	TX 48 BLDC motor power at maximum torque
R_{Cx}	Reaction force on the vertical plane (N)
R_{Cz}	Reaction force on the horizontal plane (N)
sf	Safety factor
v	Average velocity of chain
x	Radial loading factor

ДИЗАЈН, РАЗВОЈ И ИЗРАДА МАЛОГ ЕЛЕКТРОМОТОРНОГ ДИНАМОМЕТРА

Т.Д. Хонг, Ф.Т. Труонг, М.К. Фам, Н.М. Хо, Х.М.Д. Ле, Т.В. Ву

Проучавање перформанси електричних возила, радног домета и алгоритама управљања још увек је ограничено у земљама у развоју јер захтева специјализовану опрему, док се електрична возила све више користе, као што су електрични аутомобили, електрични мотори, електрични бицикли, итд. Овај рад представља дизајн и производња малог електромоторног динамометра, посебно мотора у точковима. На основу перформанси електромотора и карактеристика алтернатора, ланчани погон је пажљиво анализиран и дизајниран да истражи различите карактеристике брзине електромотора у њиховом читавом радном опсегу. Посебно у овој студији, ланчани погон има три степена са преносним односима од 1/4, 1/3 и 1/2,5. Осим тога, контролер који може аутоматски подесити ниво електричног оптерећења како би одредио различите карактеристике мотора под константним оптерећењем и поставкама гаса је такође дизајниран да контролише динамометар и прикупља основне податке. Штавише, графички кориснички интерфејс је направљен да управља динамометром брзо и флексибилно. Са флексибилним преносним односом и свеобухватном контролом алгоритма, динамометар може да истражује различите карактеристике електромотора који се користе за популарне мотоцикле и бицикле снаге до 3000В. Дизајнирани динамометар не само да има компактан дизајн, стабилан рад и прис–тупачну цену, већ је и једноставан за склапање, рад и одржавање. Ови налази се могу применити на развој динамометра за истраживање перформанси електромотора и његовог помоћног система, слу–жећи процесу истраживања и развоја електричних мотоцикала који се данас користе у земљама у развоју.